Deconfined Criticality in the Frustrated Heisenberg Honeycomb Antiferromagnet

R. Ganesh,[1] Jeroen van den Brink,[1,2] and Satoshi Nishimoto[1]

[1]*Institute for Theoretical Solid State Physics, IFW Dresden, PF 270116, D-01171 Dresden, Germany*
[2]*Department of Physics, Technical University Dresden, D-1062 Dresden, Germany*

(Received 17 January 2013; published 18 March 2013)

Using the density matrix renormalization group, we determine the phase diagram of the spin-1/2 Heisenberg antiferromagnet on a honeycomb lattice with a nearest-neighbor interaction J_1 and a frustrating, next-nearest-neighbor exchange J_2. As frustration increases, the ground state exhibits Néel, plaquette, and dimer orders, with critical points at $J_2/J_1 = 0.22$ and 0.35. We observe that both the spin gap and the corresponding order parameters vanish *continuously* at *both* the critical points, indicating the presence of deconfined quantum criticality.

DOI: 10.1103/PhysRevLett.110.127203 PACS numbers: 75.10.Jm, 75.10.Kt

Introduction.—Frustrated magnetism on the honeycomb lattice has lately received tremendous interest. This interest stems from sign-problem-free quantum Monte Carlo studies suggesting the presence of a spin-liquid phase in the honeycomb Hubbard model [1,2]. Approaching from the strong coupling side, the physics for some intermediate values of the Hubbard interaction U can be described by the spin-1/2 Heisenberg model characterized by an antiferromagnetic interaction J_1 between neighboring spins and a frustrating, next-nearest-neighbor exchange J_2 [3]. This J_1-J_2 model has emerged as an interesting Hamiltonian in its own right and as relevant to the physics of honeycomb lattice materials such as $Bi_3Mn_4O_{12}(NO_3)$ [4–6]. In this model, when the frustrating coupling J_2 is small, the well-known Néel ordered state is stable. But, at a critical value of $\alpha = J_2/J_1$, it gives way to another, possibly liquid, phase. While all studies so far agree upon the presence of a phase transition, the nature of this intermediate phase that is reached by the transition out of the Néel state is heavily debated. The intermediate phase has been identified as a Z_2 spin liquid by some [7–9] and as a plaquette resonating valence bond (pRVB) state, breaking translational symmetry, by others [10–12]. A recent variational calculation argues instead that the intermediate state does not have plaquette order [13]. Upon further increasing the frustration parameter α, all studies show a second transition into a ground state that breaks lattice rotational symmetry but may or may not have magnetic order.

We analyze this complex situation by formulating and answering four succinct fundamental questions on the J_1-J_2 honeycomb Heisenberg model. (i) As to the Néel state, do quantum fluctuations tend to stabilize or destroy it? In other words, does Néel order vanish above or below the classical threshold of $\alpha = 1/6$? (ii) What is the nature of the intermediate state? Is it a liquid state or does it have plaquette order? (iii) What is the ground state for large α? Does it have magnetic order? (iv) What is the nature of the two phase transitions? Do the order parameters develop discontinuously or continuously across the quantum critical points?

We use nominally exact two-dimensional density matrix renormalization group (DMRG) calculations to settle these issues and establish that (i) Néel order is stabilized beyond the classical limit, up to $\alpha_{c1} = 0.22$, (ii) the intermediate state has weak plaquette order with f-wave symmetry, and (iii), for $\alpha_{c2} > 0.35$, the ground state has dimer order and breaks lattice rotational symmetry. These results are summarized in the phase diagram shown in Fig. 1. Moreover, we find that, within numerical precision, (iv) both the spin gap and the relevant order parameters vanish continuously, at both critical points α_{c1} and α_{c2}. This implies that, even if two different symmetries are broken on either side of α_c, the transition is *not* first order, as one would expect from a Ginzburg-Landau-type theory. We have two second-order transitions involving Néel, plaquette, and dimer phases; the critical theories for these transitions must be unusual and not described in terms of order parameter fields. This indicates instead the presence of two deconfined quantum critical points [14,15].

Frustrated honeycomb heisenberg model.—The Hamiltonian corresponding to the J_1-J_2 Heisenberg model on a honeycomb lattice is

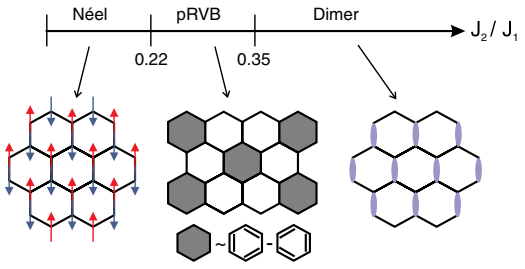

FIG. 1 (color online). Phase diagram of the spin-1/2 Heisenberg antiferromagnet on the honeycomb lattice with a nearest-neighbor interaction J_1 and a frustrating, next-nearest-neighbor exchange J_2 as obtained from DMRG calculations.

$$H = J_1 \sum_{\langle ij \rangle} \mathbf{S}_i \cdot \mathbf{S}_j + J_2 \sum_{\langle\langle ij \rangle\rangle} \mathbf{S}_i \cdot \mathbf{S}_j, \quad (1)$$

where $\langle ij \rangle$ and $\langle\langle ij \rangle\rangle$ denote nearest-neighbor and next-nearest-neighbor sites i and j, respectively, and $\alpha = J_2/J_1$ parametrizes the strength of the frustration. We consider antiferromagnetic coupling: J_1, J_2, and α are all positive. The model is well understood in the classical limit: At the critical value of $\alpha = 1/6$, the ordering wave vector smoothly moves away from the Néel wave vector to give an incommensurate spiral [16]. This spiral state exhibits interesting order-by-disorder physics [6,16]. However, in the extreme quantum limit of $S = 1/2$, the phase diagram is not well established [7–13]. We use the DMRG method to resolve this issue.

Method.—Our DMRG is truly two dimensional—we consider clusters with geometries chosen to be conducive to various ordering patterns. It is well known that one can lift the degeneracy of wave functions by taking some or all edges to be open. We use appropriate edge geometries as weak perturbing fields to induce symmetry breaking in the ground state. By performing measurements in the center of the cluster, one can estimate the order parameter induced by the edge geometry. Upon systematically increasing the size of the system, the effect of the edges becomes progressively weaker, and thus, by scaling to the thermodynamic limit, we can obtain the value of the order parameter in the ground state. In all cases, we have obtained smooth finite-size scaling, which indicates that our results exhibit a steady convergence to the thermodynamic limit.

As described below, we have used a variety of cluster geometries appropriate for each phase. Note that the performance of DMRG calculation is equally stable for any ordered phase at $\alpha < \mathcal{O}(1)$. We study several cluster sizes with a total number of sites up to 96 and keep up to 6000 density matrix eigenstates in the renormalization procedure. We perform ~ 10 sweeps until the ground-state energy converges within an error of $\sim 10^{-5} J_1$. All quantities calculated in this Letter have been extrapolated to the limit $n \to \infty$, where n is the number of retained eigenstates.

Quantum stabilization of Néel order.—We first determine the value of α at which Néel order vanishes and establish the role of quantum fluctuations in this process. Naïvely, one expects quantum fluctuations to destabilize Néel order for $S = 1/2$, thereby pushing the α_{c1} to a value below $1/6$. On the other hand, as the Néel state is collinear, quantum fluctuations may prefer the Néel state over a competing spiral phase and push α_{c1} above $1/6$. Even though various approaches have been used to address this issue, a consistent picture has not emerged so far. Calculations which support the hypothesis that $\alpha_{c1} < 1/6$ include linear spin-wave theory [17], a one-loop renormalization group study of the nonlinear sigma model [18], functional renormalization group analysis [19], and a variational Monte Carlo approach using resonating valence bond and Huse-Elser wave functions [9]. On the other hand, approaches which support the $\alpha_{c1} > 1/6$ hypothesis include exact diagonalization [10,11], Schwinger boson mean-field theory [17,20], series expansions [21], coupled-cluster calculations [12], and a variational Monte Carlo calculation using entangled plaquette states [13].

The DMRG results presented in Fig. 2 conclusively establish that quantum fluctuations stabilize Néel order beyond the classical regime of stability. We have used two cluster geometries—diamond and hexagonal [Figs. 2(a) and 2(b)]. One should be aware that periodic boundary conditions in some direction artificially enhance or diminish Néel correlations due to short-range periodicity. This finite-size effect decays only slowly with increasing cluster size. To circumvent this issue, we keep all edges of the clusters open and measure the following order parameter as a function of α:

$$m^2(N) = \frac{1}{N}\left(\sum_i (-1)^i \vec{S}_i\right)^2. \quad (2)$$

As shown in Fig. 2, this quantity shows good finite-size scaling with terms proportional to $1/L$ and $1/L^2$, where L is the linear extent of the system. In the unfrustrated situation ($\alpha = 0$), the staggered moment m in the thermodynamic limit comes out to be 0.2857 ± 0.039, which is consistent

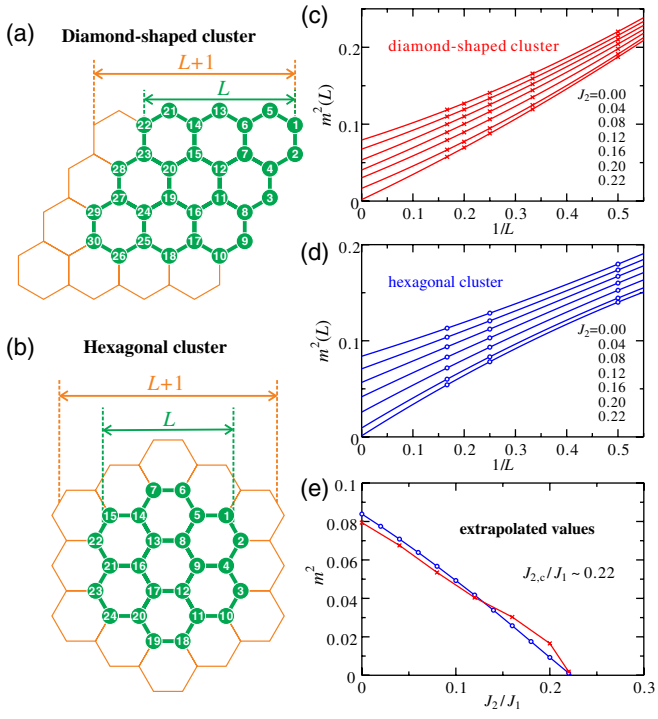

FIG. 2 (color online). Finite-size scaling of the Néel order parameter. (a) Diamond cluster with $L = 3$. (b) Hexagonal cluster with $L = 3$. (c),(d) Finite-size scaling of the Néel order parameter defined in Eq. (2) for diamond and hexagonal clusters. (e) Scaled Néel order parameter as a function of $\alpha = J_2/J_1$ for diamond (closed red circles) and hexagonal (open blue circles) clusters.

with previously estimated values of 0.2677(6) and 0.270 obtained from quantum Monte Carlo calculations [22] and exact diagonalization [11], respectively. As α increases, the obtained value of the Néel order parameter steadily decreases. At the critical value of $\alpha_{c1} \sim 0.22$, we observe that Néel order vanishes in a continuous transition, as shown in Fig. 2(e). Both diamond and hexagonal cluster geometries give the same value of α_{c1}, which signals the robustness of our result. Thus, quantum fluctuations stabilize Néel order significantly beyond the classical threshold.

Nonlinear spin-wave analysis.—The excitations of the Néel state are well captured by spin-wave theory, which treats quantum fluctuations using an expansion in powers of S. Linear spin-wave theory with $\mathcal{O}(S^1)$ terms gives $\alpha_{c1} \sim 0.11$ [17], which is *below* the classical threshold. To reconcile this with the observed DMRG phase boundary, we take into account the quartic spin-wave interaction terms of order $\mathcal{O}(S^0)$. We treat the interactions at mean-field level (for details, see the Supplemental Material [23]) and observe that the Hartree-Fock parameters merely renormalize the strength of the J_1 and J_2 couplings. This effectively scales the frustration parameter $\alpha = J_2/J_1$ down so that the Néel state only becomes unstable beyond $\alpha \sim 0.214$. The quartic terms thereby provide a significant correction to the critical frustration ratio. The precise value of α_{c1} may depend upon further corrections beyond quartic order. Nevertheless, nonlinear spin-wave analysis confirms the strong tendency for quantum fluctuations to stabilize Néel order beyond the classical limit.

Intermediate plaquette phase.—We observe the presence of an intermediate pRVB phase, as suggested previously [10–12,24], for $0.22 \lesssim \alpha \lesssim 0.35$. In an earlier report, we had suggested f-wave pRVB order based on a plaquette operator analysis [25]. This state consists of a $\sqrt{3} \times \sqrt{3}$ arrangement of plaquettes, as shown in Fig. 1—each shaded plaquette is in an antisymmetric combination of the two Kekulé singlet covers. To test for plaquette order in the ground state, we choose the cluster geometry shown in Fig. 3(a) which favors plaquette order (this also favors columnar dimer order [26], but we have explicitly checked that it does not occur). This choice of boundary conditions acts as a weak field which induces plaquette ordering, as shown by the shaded hexagons in Fig. 3(a). We measure the ordering amplitude at the center of the cluster, away from the boundaries. To determine the pRVB order parameter, we first define the two single-plaquette states $|a\rangle$ and $|b\rangle$—the two Kekulé singlet covers of a single hexagon. The f-wave, antisymmetric, pRVB wave function is given by $|-\rangle \sim |a\rangle - |b\rangle$, up to a normalization constant. The order parameter corresponding to pRVB order is the projection onto the antisymmetric wave function: $\hat{O}_{\mathrm{pRVB}} = |-\rangle\langle -|$, acting on a shaded plaquette in Fig. 3(a). We use the closely related plaquette-flip operator which flips the two Kekulé covers:

$$\hat{P} = -|a\rangle\langle b| - |b\rangle\langle a|. \tag{3}$$

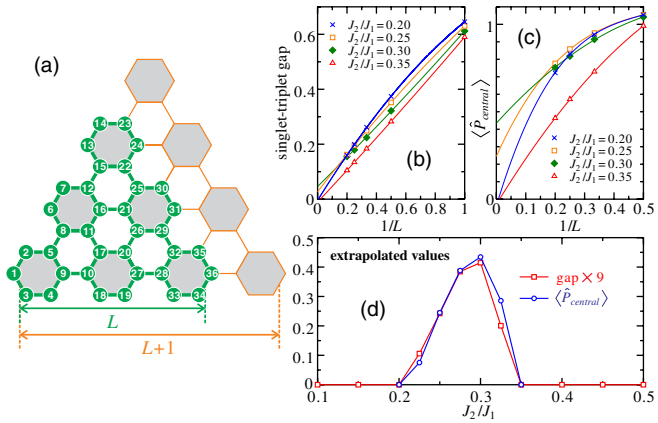

FIG. 3 (color online). (a) Cluster geometry with $L = 3$ used to establish the presence of plaquette order. (b),(c) Finite-size scaling of the spin gap and $\langle \hat{P}_{\mathrm{central}} \rangle$—a measure of pRVB amplitude. We find good scaling with polynomials up to cubic order in $1/L$. (d) Spin gap and $\langle \hat{P}_{\mathrm{central}} \rangle$ in the thermodynamic limit.

If the plaquette is in the pure $|-\rangle$ state, this operator has an expectation value of $5/4$ (see the Supplemental Material [23] for details). For the case of s-wave pRVB order (a symmetric combination of singlet covers), this expectation value would be negative.

To measure pRVB order at the cluster center, we define $\langle \hat{P}_{\mathrm{central}} \rangle$ as the average of $\langle \hat{P} \rangle$ over three plaquette ordering hexagons at the center of the system. As seen from Fig. 3(a), one cannot always identify a single central plaquette for a given L. So, we average over three plaquettes at the center of the system. Finite-size scaling of $\langle \hat{P}_{\mathrm{central}} \rangle$ provides the strength of pRVB order in the limit of infinite system size. Consistent with f-wave pRVB order, this expectation value is positive for $0.22 \lesssim \alpha \lesssim 0.35$. Figure 3(c) shows the finite-size scaling of $\langle \hat{P}_{\mathrm{central}} \rangle$, which indeed scales to a positive value in the thermodynamic limit. We also find a finite spin gap that is consistent with $\sqrt{3} \times \sqrt{3}$ plaquette ordering. We note, however, that strong quantum fluctuations reduce the amplitude of plaquette ordering: $\langle \hat{P}^{N=\infty}_{\mathrm{central}} \rangle$ reaches a maximum value of ~ 0.43 compared to $5/4$ for the case of pure pRVB order. The strength of pRVB order can also be characterized by $\bar{p}$, the amplitude of the projection onto the $|-\rangle$ plaquette wave function as defined in Ref. [25]. For decoupled hexagons in the regime $0 < \alpha < 0.5$, there is perfect pRVB order with $\bar{p} = 1$. Our DMRG results indicate that, in the honeycomb $J_1 - J_2$ model, pRVB order is strongly affected by quantum fluctuations and reduced to $\bar{p} \lesssim 0.34$. To confirm the existence of pRVB order, we also measure the spin gap which is the energy difference between the first triplet excited state and the singlet ground state,

$$\Delta(L) = E_1(L) - E_0(L), \qquad \Delta = \lim_{L\to\infty} \Delta(L), \tag{4}$$

where $E_n(L)$ is the nth eigenenergy ($n = 0$ corresponds to the ground state) of the system size L. The scaling analysis

of the finite-size data is shown in Fig. 3(b), and the results extrapolated to the thermodynamic limit are plotted in Fig. 3(d). We observe that the gap is finite only in the region of positive $\langle \hat{P}_{\text{central}} \rangle$.

Dimer phase.—At larger values of J_2, the presence of a dimer state which breaks lattice rotational symmetry has been proposed previously [16,24]. This state has been variously called the staggered valence bond solid or the nematic valence bond solid state in literature. We establish that this state occurs in the phase diagram for $\alpha \gtrsim 0.35$ using the cluster geometry in the inset of Fig. 4(a). We use open boundary conditions in the x direction and periodic boundary conditions along the y direction, thus breaking the degeneracy associated with threefold lattice rotational symmetry. The cluster favors bond ordering with horizontal dimers, as shown in Fig. 4(a). We first measure the breaking of lattice rotational symmetry by evaluating the expectation value of

$$\hat{R} = \mathbf{S}_A \cdot \mathbf{S}_B - \mathbf{S}_B \cdot \mathbf{S}_C, \tag{5}$$

where the sites A, B, and C are chosen close to the center of the system [see Fig. 4(a)]. We determine the expectation $\langle \hat{R} \rangle$ while systematically increasing system size. If the true ground state breaks lattice rotational symmetry, we expect this quantity to scale to a nonzero value in the thermodynamic limit. For finite-size scaling, we first take $L_x \to \infty$ followed by $L_y \to \infty$. This sequence of limits ensures that there is no degeneracy arising from lattice rotations. We obtain smooth finite-size scaling by restricting ourselves to even values of L_y, as shown in Fig. 4. Including odd L_y values leads to small oscillations, preventing smooth scaling.

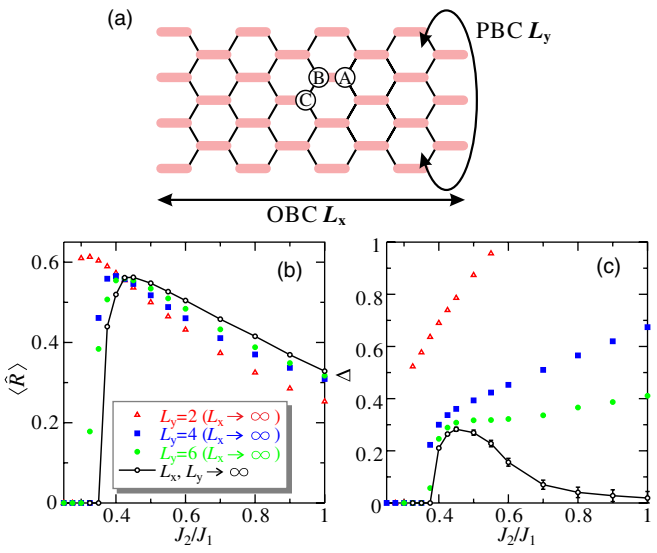

FIG. 4 (color online). (a) Cluster geometry to detect dimer order. We enforce periodic boundary conditions (PBCs) along L_y and open boundary conditions (OBCs) along L_x. (b) Finite-size scaling of $\langle \hat{R} \rangle$, with an order parameter corresponding to lattice rotational symmetry breaking. For scaling, we first take $L_x \to \infty$ and then $L_y \to \infty$. We show data points obtained by L_x scaling for different fixed L_y values. The points connected by the line are the final values obtained from L_y scaling. (c) Finite-size scaling of the spin gap (obtained by similar finite-size scaling) as a function of $\alpha = J_2/J_1$.

Figure 4(b) shows that $\langle \hat{R} \rangle$ scales to a nonzero value for $\alpha \gtrsim 0.35$, clearly establishing broken lattice rotational symmetry in the ground state. However, this is consistent with two ground state candidates—dimer order or magnetic stripe order [11]. To distinguish between these two, we measure the spin gap. The finite-size scaling for the spin gap is shown in Fig. 4(c). While first increasing L_x, we find that the spin gap scales as $1/L_x^2$. Later, upon increasing L_y, we find that the spin gap scales as a power law—$1/L^{\nu}$, with $\nu \sim 1.5$. The error bars shown in Fig. 4(c) are associated with the choice of ν to fit the data points. For $0.35 \lesssim \alpha \lesssim 0.6$, the spin gap scales to a nonzero value robustly. For $\alpha \gtrsim 0.7$, it is not possible to determine reliably whether the spin gap closes. The nonzero spin gap clearly indicates dimer order and rules out magnetic order.

Nature of phase transitions.—We have clearly demonstrated the presence of Néel, plaquette, and dimer orders. Naïvely, one expects first-order quantum phase transitions (QPTs) between these phases as they break different symmetries. Our DMRG results, however, evidence a continuous transition out of the Néel phase: As can be seen from Fig. 2, the Néel order parameter vanishes continuously at $\alpha_{c1} = 0.22$. This implies the presence of an exotic deconfined QPT [12,27]. Approaching from the Néel side, tripled monopoles are allowed, leading to a field theory of the type discussed in Refs. [14,28], whereas, approaching from the pRVB side, the quantum field theory governing this deconfined transition must involve spinons coupled to vortices in the pRVB order parameter [26]. This is an exciting proposition, as a deconfined QPT in a model with realistic Heisenberg interactions has not been identified before. Surprisingly, DMRG results suggest that the plaquette-dimer transition is also continuous. As seen from Fig. 3(d) and Fig. 4, at $\alpha_{c2} = 0.35$, there is no evidence for either plaquette ordering or breaking of lattice rotational symmetry. More work is needed to study the vicinity of these transitions, to extract critical exponents, and to rule out weak first-order behavior or the presence of a small intervening phase. If there is indeed a continuous transition between dimer and plaquette phases, it would be yet another Landau-forbidden QPT within the same model. The field theory corresponding to this transition would be of immense interest.

We thank Subir Sachdev and Kai Schmidt for stimulating comments and Ioannis Rousochatzakis for many useful discussions.

Note added.—During the preparation of this manuscript, a DMRG study in Ref. [29] reported a similar sequence of Néel, plaquette, and dimer orders as well as the continuous nature of the transition out of the Néel phase.

[1] Z. Y. Meng, T. C. Lang, S. Wessel, F. F. Assaad, and A. Muramatsu, Nature (London) **464**, 847 (2010).
[2] S. Sorella, Y. Otsuka, and S. Yunoki, Sci. Rep. **2**, 992 (2012).
[3] H. Y. Yang and K. P. Schmidt, Europhys. Lett. **94**, 17 004 (2011).
[4] H. C. Kandpal and J. van den Brink, Phys. Rev. B **83**, 140412 (2011).
[5] R. Ganesh, D. N. Sheng, Y.-J. Kim, and A. Paramekanti, Phys. Rev. B **83**, 144414 (2011).
[6] S. Okumura, H. Kawamura, T. Okubo, and Y. Motome, J. Phys. Soc. Jpn. **79**, 114705 (2010).
[7] F. Wang, Phys. Rev. B **82**, 024419 (2010).
[8] Y.-M. Lu and Y. Ran, Phys. Rev. B **84**, 024420 (2011).
[9] B. K. Clark, D. A. Abanin, and S. L. Sondhi, Phys. Rev. Lett. **107**, 087204 (2011).
[10] H. Mosadeq, F. Shahbazi, and S. A. Jafari, J. Phys. Condens. Matter **23**, 226006 (2011).
[11] A. F. Albuquerque, D. Schwandt, B. Hetényi, S. Capponi, M. Mambrini, and A. M. Läuchli, Phys. Rev. B **84**, 024406 (2011).
[12] R. Bishop, P. Li, D. Farnell, and C. Campbell, J. Phys. Condens. Matter **24**, 236002 (2012).
[13] F. Mezzacapo and M. Boninsegni, Phys. Rev. B **85**, 060402 (2012).
[14] T. Senthil, A. Vishwanath, L. Balents, S. Sachdev, and M. Fisher, Science **303**, 1490 (2004).
[15] C. Xu, Int. J. Mod. Phys. B **26**, 1230007 (2012).
[16] A. Mulder, R. Ganesh, L. Capriotti, and A. Paramekanti, Phys. Rev. B **81**, 214419 (2010).
[17] A. Mattsson, P. Fröjdh, and T. Einarsson, Phys. Rev. B **49**, 3997 (1994).
[18] T. Einarsson and H. Johannesson, Phys. Rev. B **43**, 5867 (1991).
[19] J. Reuther, D. A. Abanin, and R. Thomale, Phys. Rev. B **84**, 014417 (2011).
[20] H. Zhang and C. A. Lamas, Phys. Rev. B **87**, 024415 (2013).
[21] J. Oitmaa and R. R. P. Singh, Phys. Rev. B **84**, 094424 (2011).
[22] E. V. Castro, N. M. R. Peres, K. S. D. Beach, and A. W. Sandvik, Phys. Rev. B **73**, 054422 (2006).
[23] See Supplemental Material at http://link.aps.org/supplemental/10.1103/PhysRevLett.110.127203 for (i) details of nonlinear spin-wave analysis; (ii) the definition of our plaquette-flip operator and its expectation values.
[24] J. Fouet, P. Sindzingre, and C. Lhuillier, Eur. Phys. J. B **20**, 241 (2001).
[25] R. Ganesh, S. Nishimoto, and J. van den Brink, Phys. Rev. B **87**, 054413 (2013).
[26] C. Xu and L. Balents, Phys. Rev. B **84**, 014402 (2011).
[27] D. J. J. Farnell, R. F. Bishop, P. H. Y. Li, J. Richter, and C. E. Campbell, Phys. Rev. B **84**, 012403 (2011).
[28] N. Read and S. Sachdev, Phys. Rev. B **42**, 4568 (1990).
[29] Z. Zhu, D. A. Huse, and S. R. White, this issue, Phys. Rev. Lett. **110**, 127205 (2013).